Anglo–French Physical Acoustics Conference 2009 IOP Publishing
Journal of Physics: Conference Series **195** (2009) 012008 doi:10.1088/1742-6596/195/1/012008

The effects of nonlinear wave propagation on the stability of inertial cavitation

D Sinden, E Stride & N Saffari

Mechanical Engineering, Roberts Building, Torrington Place, London, WC1E 7JE, United Kingdom

E-mail: d.sinden@ucl.ac.uk

Abstract. In the context of forecasting temperature and pressure fields generated by high-intensity focussed ultrasound, the accuracy of predictive models is critical for the safety and efficacy of treatment. In such fields 'inertial' cavitation is often observed. Classically, estimations of cavitation thresholds have been based on the assumption that the incident wave at the surface of a bubble is the same as in the far-field, neglecting the effect of nonlinear wave propagation. By modelling the incident wave as a solution to Burgers' equation using weak shock theory, the effects of nonlinear wave propagation on inertial cavitation are investigated using both numerical and analytical techniques. From radius-time curves for a single bubble, it is observed that there is a reduction in the maximum size of a bubble undergoing inertial cavitation and that the inertial collapse occurs earlier in contrast with the classical case. Corresponding stability thresholds for a bubble whose initial radius is slightly below the critical Blake radius are calculated, providing a lower bound for the onset of instability. Bifurcation diagrams and frequency-response curves are presented associated with the loss of stability. The consequences and physical implications of the results are discussed with respect to the classical results.

1. Introduction

For materials with a nonlinear stress-strain relationship, such as tissue [1], the point of maximum compression for a wave may propagate faster than the point of maximum rarefaction, leading to a distortion in the wave profile and the redistribution of energy from the fundamental harmonic frequency to higher harmonics. The pressures associated with therapeutic high intensity focused ultrasound (HIFU) may be high enough for the effects of nonlinear wave propagation to be significant [2]. As high frequency components are absorbed more easily than those with lower frequencies, nonlinear wave propagation contributes to increased absorption, enhanced heating and a subsequent shift in the focal point of targeted ultrasonic beam, potentially damaging healthy tissue. As well as providing greater predictive accuracy, knowledge of nonlinear wave propagation will enable increased accuracy in calibration using the received signal generated by bubble oscillations [3] and thus greater accuracy in treatment procedures. However, in this paper the implications of nonlinear wave propagation on inertial cavitation are investigated and stability criteria re-derived in an attempt to reconcile theory and experiment.

The Rayleigh-Plesset equation [4] is a nonlinear equation which determines the size of a spherical bubble subject to a varying pressure field. Wave propagation from the far-field to the surface of the bubble is generally assumed to be linear, yet this does not correspond with experimental observations in the context of high intensity focused ultrasound. Moss [5]

attempted to incorporate the effects of boundary conditions and global compressibility/local incompressibility into the Rayleigh-Plesset equation but only considered linear wave propagation. The equation derived was identical to the classical Rayleigh-Plesset equation if the far-field pressure is replaced by an attenuated pressure measured within 25 bubble radii of the bubble surface. In this paper the effect of distortion rather than attenuation of the wave profile and its effect on the stability of oscillations will be investigated.

Lauterborn and co-workers [4,6] and Smerka [7] showed experimentally and numerically that bubble oscillations undergo a sequence of period-doubling bifurcations leading to unstable quasi-periodic (chaotic) oscillations. The period doubling route to chaos occurs through a succession of saddle-node bifurcations of subharmonic periodic orbits. Homoclinic bifurcations are the limit of a countable sequence of subharmonic saddle-node bifurcations and thus provide an insight into the parameters regimes at which unbounded growth occurs.

Mel'nikov's method provides a measure of the distance between the stable and unstable manifolds of a periodically perturbed system [8]. If the manifolds intersect transversely once, they will intersect transversely infinitely many more times. The transverse intersections can be represented by Smale horseshoes, through which the Smale-Birkhoff theorem give an elegant description of sensitivity to initial conditions and the resulting chaotic oscillations. Hence the Mel'nikov criteria marks the first event in a sequence of events leading to unbounded bubble growth and as such provides a valuable lower bound threshold.

The first application of Mel'nikov's method to cavitation was performed by Chang and Chen [9] on the effect of viscosity on the Hamiltonian structure. Szeri [10] computes the first-order splitting for the Rayleigh-Plesset equation numerically. Harkin [11] performs Mel'nikov analysis analyically on bubbles whose initial radius is slightly smaller than Blake critical radius. Using matched perturbation analysis, Harkin derives a second order normal form for the Rayleigh-Plesset equation. The normal form is a damped driven oscillator. An escape velocity, like the static Blake criterion, provides an upper bound for when unbounded growth will occur, whereas Mel'nikov's method provides a lower bound for when the transition to chaos and unbounded growth may occur. The fate of bubbles whose initial conditions lie in the intermediate region between the Mel'nikov and Blake thresholds can be computed by a transport-type processes [12]. A Bernoulli shift map on two symbols has already been constructed numerically from a bifurcation diagram for the full Rayleigh-Plesset equation [13] without explicit inference to sensitivity to initial conditions. In each application of Mel'nikov's method the incident pressure wave was sinusoidal [7, 9, 11, 10]. In this paper the analysis is performed for nonlinear waves.

The outline of this paper is as follows, in section 2 nonlinear wave propagation is considered and wave profiles derived. Then in section 3 the Rayleigh-Plesset equation is introduced and the effects of nonlinear wave propagation investigated. In section 4 Mel'nikov analysis is performed for nonlinear wave propagation, providing an improved measure of the values at which quasi-periodic oscillation and unbounded growth may occur. Finally, conclusions and implications are discussed in section 5.

2. Nonlinear Wave Propagation

There is no universally accepted system of partial differential equations for the modelling of ultrasound propagation in biological tissue. Perhaps the best known is the Khokhlov-Zabolotskaya-Kuznetsov (KZK) equation. The KZK equation is a parabolic wave equation which includes the effects of diffraction, absorption and nonlinearity of the directed beams [3]. The KZK equation for an axi-symmetric beam which propagates in the r direction is written in terms of the acoustic pressure $p\,(r,t)$ as

$$\frac{\partial^2 p}{\partial r \partial t'} = \frac{c_0}{2}\nabla_\perp^2 p + \frac{D}{2c_0^2}\frac{\partial^3 p}{\partial t'^3} + \frac{\beta}{2\rho c_0^3}\frac{\partial^2 p^2}{\partial t'^2} \tag{1}$$

where c_0 is the initial wave speed, ρ is the density of the medium, β is the standard nonlinearity coefficient given by $\beta = 1 + B/2A$, where B/A is the standard nonlinearity parameter, D is the sound diffusivity and $t' = t - r/c_0$ is the retarded time variable. The Laplacian is taken with respect to the transverse coordinates. The sound diffusivity is given by

$$D = \frac{1}{\rho}\left(\mu_b + 4\mu_s/3 + \kappa\left(1/c_v - 1/c_p\right)\right)$$

where μ_b and μ_s are the bulk and shear viscosities respectively, $1 \leq \kappa \leq \gamma$ the polytropic exponent, and c_v and c_p are the specific heat capacities at constant volume and pressure respectively. If $\kappa = 1$ the system is isothermal, if $\kappa = \gamma \equiv c_p/c_v$ the system is adiabatic. In the study of cavitation it will be assumed that the bubble is essentially stationary over the time scales considered and that the distance from the surface of the bubble to the shock front is constant, so that r is a fixed value at the surface of the bubble. The equation (1) can be integrated with respect to retarded time to give

$$\frac{\partial p}{\partial r} = \frac{c_0}{2}\int_{-\infty}^{t'} \nabla_\perp^2 p\left(s,t\right)\,\mathrm{d}s + \frac{D}{2c_0^2}\frac{\partial^2 p}{\partial t'^2} + \frac{\beta}{2\rho c_0^3}\frac{\partial p^2}{\partial t'}. \tag{2}$$

Discarding the effects of diffraction Burgers', or alternatively the Burgers-Hopf, equation is recovered

$$\frac{\partial p}{\partial r} = \frac{D}{2c_0^2}\frac{\partial^2 p}{\partial t'^2} + \frac{\beta}{2\rho c_0^3}\frac{\partial p^2}{\partial t'}. \tag{3}$$

If $D = 0$ the fluid is inviscid, and the so-called lossless Burgers equation is recovered.

From a given driving pressure, $f\left(t\right)$, the incident pressure wave, $p\left(t\right)$, can be expressed using weak shock theory. The location of a shock is determined by the Rankine-Hugoniot relation defining the conservation of flux. The areas enclosed by the multi-valued solution to the left and right of the shock are equal. Thus, by this symmetry, the shock is positioned at the zero of the linear solution. For a sinusoidal driving pressure of magnitude P and frequency ω, i.e.

$$f = P\sin\left(\omega t\right), \tag{4}$$

a Fourier expansion of the solution to the lossless Burgers equation yields the Bessel-Fubini or alternately the Fubini solution

$$p = \frac{2P}{r_s}\sum_{n=1}^{\infty}\frac{1}{n}J_n\left(nr_s\right)\sin\left(\omega_n t'\right), \tag{5}$$

where $\omega_n = n\omega$, J_n is an n^{th}-order Bessel functions of the first kind and r_s is the normalised distance to a shock given by

$$r_s = \frac{r}{r_c} \quad \text{where} \quad r_c = \frac{\rho c_0^3}{\beta\omega P}$$

is the location of the shock.

Beyond the shock, weak shock theory can once again be employed to find a solution, however, the resulting analytical solution takes an integral form. An asymptotic solution, valid for, say $r_s > 3$, is

$$p = \frac{2P}{1 + r_s}\sum_{n=1}^{\infty}\frac{1}{n}\sin\left(\omega_n t'\right). \tag{6}$$

which can be expressed in the time domain as

$$p = \begin{cases} -\dfrac{P\left(\omega t' + \pi\right)}{1 + r_s} & \text{for} \quad -\pi < \omega t' < 0, \\ -\dfrac{P\left(\omega t' - \pi\right)}{1 + r_s} & \text{for} \quad 0 < \omega t' < \pi. \end{cases}$$

A general solution to the Burgers'-Hopf equation for a sinusoidal driving pressure (4), derived by transforming the nonlinear equation into a linear diffusion equation via the Hopf-Cole transformation, is given by

$$p = -\frac{4P}{\kappa} \frac{\sum_{n=1}^{\infty} n\left(-1\right)^n I_n\left(\Gamma/2\right) e^{-n^2 r_s/\Gamma} \sin\left(\omega_n t'\right)}{I_0\left(\Gamma/2\right) + 2\sum_{n=1}^{\infty}\left(-1\right)^n I_n\left(\Gamma/2\right) e^{-n^2 r_s/\Gamma} \cos\left(\omega_n t'\right)} \tag{7}$$

where I_n is an n^{th}-order modified Bessel functions of the first kind and Γ is the Gol'dberg number which relates the importance of nonlinear effects against dissipative effects as

$$\Gamma = \frac{2\beta P}{D\rho\omega}.$$

If $\Gamma \gg 1$ then the relative effects of nonlinearity are strong, if $\Gamma < 1$ the relative effects of nonlinearity are weak.

Unlike the Fubini solution (5), for strong nonlinearity, i.e. $\Gamma \gg 1$, the solution converges slowly but far from the shock, i.e. again say $r_s > 3$, asymptotic analysis yields the more usable formulation

$$p = \frac{2P}{\Gamma} \sum_{n=1}^{\infty} \frac{\sin\left(\omega_n t'\right)}{\sinh\left(n\left(1 + r_s\right)/\Gamma\right)} \tag{8}$$

called the Fay solution. The Fay solution can be expressed as the periodic function

$$p = \frac{P}{1 + r_s}\left(-\omega t' + \pi \tanh\left(\frac{\pi\Gamma\omega t'}{2\left(1 + r_s\right)}\right)\right) \quad -\pi \le \omega t' \le \pi.$$

In the lossless limit as viscosity vanishes, that is as $\Gamma \to \infty$, the Fay solution recovers the Fourier expression for a sawtooth function (6). The Fubini (5) and Fay (8) solutions may at first seem incompatible but each holds in a different region of the flow; the Fubini solution close to the source as a shock begins to form and the Fay solution far from the source as a shock begins to decay. Blackstock [14] shows that the true solution to the lossless Burgers equation over the entire domain is simply the sum of the two solutions (5) and (6). In the near-field the Fubini solution is dominant, in the far-field the sawtooth solution is dominant. In [15] exact solutions of Burgers' equation from the Cole-Hopf transformation were computed numerically and contrasted against the analytical solutions and showed good agreement between the sets of solutions unless in the immediate neighbourhood of the shock. The formation of a shock will occur in a region of peak negative pressure and hence is a prime site for the nucleation of cavities. Thus the forthcoming analysis will be performed either before a shock or significantly after, so that only the effect of nonlinear wave propagation on pre-existing cavities is studied.

Figure 1 presents nonlinear wave profiles (5) and a linear wave profile (4) illustrating the distortion due to nonlinear propagation of waves with equal amplitude. Throughout this paper comparisons between linear and nonlinear waves of equal amplitude are studied.

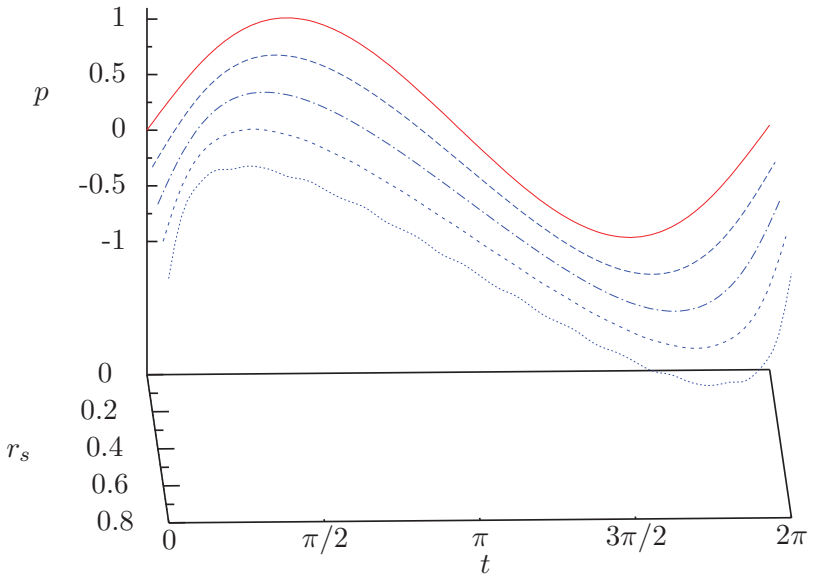

Figure 1. Profiles of incident waves for linear and nonlinear wave propagation as the distance from a shock front decreases. The nonlinear waves are modeled by the first twenty terms of the (normalised) Fubini solution. The linear wave is modelled when $r = 0$ (red,solid), nonlinear waves are $r_s = 1/5$ (blue, dashed), $r_s = 2/5$ (blue, dot-dashed), $r_s = 3/5$ (blue, short-dashed) and $r_s = 4/5$ (blue, dot).

3. Rayleigh-Plesset Equation

The Rayleigh-Plesset equation is an ordinary differential equation which models the oscillations of a spherical bubble of radius $R = R(t)$ whose centre is stationary. The Rayleigh-Plesset equation can be derived by balancing the energy supplied to the bubble by the incident pressure and the surrounding fluid and the kinetic energy of the bubble oscillations [16] yielding

$$\rho\left(R\ddot{R} + \frac{3}{2}\dot{R}^2\right) = p_g(R) + p_v - p_\infty + p(t) + \frac{2\sigma}{R} + \frac{4\mu\dot{R}}{R} \tag{9}$$

where p_g is the internal pressure of the gas in the bubble given by the hard-core van der Waals relationship

$$p_g(R(t)) = \left(p_\infty - p_v + \frac{2\sigma}{R_0}\right)\left(\frac{R_0^3 - a^3}{R(t)^3 - a^3}\right)^\kappa \tag{10}$$

with R_0 the equilibrium radius, a the van der Waals hard-core radius, p_v the vapour pressure, p_∞ is the ambient pressure, σ is the surface tension and μ viscosity. The gas is assumed to be ideal as the internal pressure is a function of the bubble radius only. The forcing pressure will

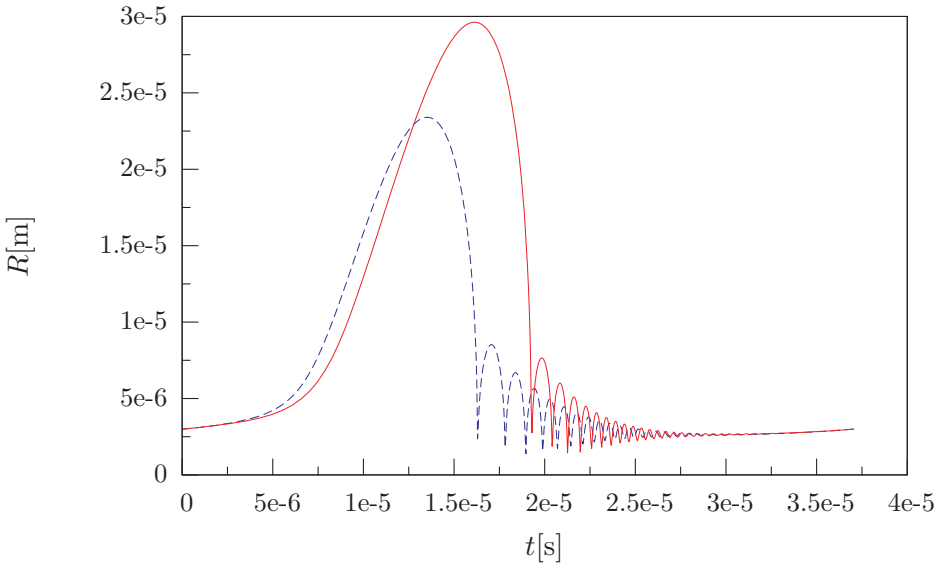

Figure 2. Contrasting profiles of inertial cavitation for linear (red, solid) and nonlinear (blue, dashed) wave propagation modeled by the first ten terms of the Fubini solution. $R_0 = 0.6\mu$m, subject to a wave with frequency $\omega = 2\pi \cdot 26$kHz, amplitude of driving pressure $P = 1.36$atm, normalised distance to the shock $r_s = 1/20$ ambient pressure $p_\infty = 1$atm, surface tension $\sigma = 0.073\text{kgm}^{-2}$, viscosity $\mu = 10^{-3}\text{kgm}^{-1}\text{s}^{-1}$, density $\rho = 1000\text{kgm}^{-3}$, polytropic exponent $\kappa = 5/3$ and hard-core radius $a = R_0/8.85$.

take the form

$$p(t) = \sum_{n=1}^{\infty} P_n \sin(\omega_n (t + t_0))$$

where P_n are the Fourier terms of a solution to a Burgers' equation, such as those given by the Fubini (5) or the Fay (8) solutions.

Figure 2 contrasts the effects of nonlinear and linear wave propagation. It is clear that for nonlinear wave propagation inertial cavitation occurs before and at a smaller maximum radius than for linearly propagated waves. This has two significant effects, firstly as the collapse occurs at a small maximum radius there is a diminished chance of shape instability [17] and secondly, as the collapse occurs earlier more after-bounces can occur so that the bubble returns to a stable initial radius before the next cycle begins. Note that the period of the after-bounces is the same for the nonlinear and linear wave since the after-bounces occur at the natural frequency of the Rayleigh-Plesset equation which is independent of the applied pressure.

4. Mel'nikov Analysis

Considering an unforced bubble and let $R(t) = R_0(1 + x)$. When $x \ll 1$ then to first order the nondimensional Rayleigh-Plesset equation yields the simple harmonic equation

$$\ddot{x} + \omega_0 x = 0 \quad \text{where} \quad \omega_0^2 = \frac{1}{\rho}\left(\frac{3\kappa(p_\infty - p_v)R_0}{R_0^3 - a^3} + 2\sigma\left(\frac{3\kappa}{R_0^3 - a^3} - \frac{1}{R_0^3}\right)\right). \tag{11}$$

The natural frequency ω_0 is used to nondimensionalise time by $\tau = \omega_0 t$ so that the new time-like variable will be a function of the perturbation parameter. Note that when $a = 0$ and $\kappa = 1$ then the frequency given by Harkin [11, Eq. (12)] is recovered. In this section Harkin's analysis is

followed as it gives an analytical expression for the transverse intersections which allows for direct comparison between linear and nonlinear wave propagation.

The static Blake threshold pressure is the point at which the internal pressure $p_v + p_g$ is equal to the external pressure $p_l + 2\sigma/R$, thus for internal pressures larger than this threshold unbounded growth will occur. The equilibrium pressure exerted on the bubble surface by the liquid, p_l, is given by

$$p_l = p_g + p_v - \frac{2\sigma}{R}. \tag{12}$$

Now perturb the equilibrium radius by $R(t) = R_0(1 + \epsilon x(\tau))$ with ϵ a small parameter given by

$$\epsilon = 2(1 - R_0/R_c)$$

where $R_c = R_c\left(\tilde{G}, \sigma, \kappa, a\right)$ is the Blake critical radius, found as the stationary solutions to the unforced Rayleigh-Plesset equation

$$\frac{3\kappa\tilde{G}R^4}{(R^3 - a^3)^{(\kappa+1)}} = 2\sigma \quad \text{where} \quad \tilde{G} = \left(p_\infty - p_v + \frac{2\sigma}{R_0}\right)\left(R_0^3 - a^3\right)^\kappa. \tag{13}$$

Unfortunately if $a \neq 0$ then there is no simple analytical expression for the critical Blake radius. In the isothermal case the critical radius can be found explicitly as the solution to the cubic equation

$$R^3 - \sqrt{\frac{3\tilde{G}}{2\sigma}}R^2 - a^3 = 0.$$

It is straightforward to show from the discriminant of the cubic equation when $a \geq 0$ and $\tilde{G} \geq 0$ that the equation will have one real solution and a pair of ignorable complex conjugate solutions. In the case of no hard-core radius, i.e. $a = 0$, then

$$R_c = \sqrt[3\kappa-1]{\frac{3\kappa\tilde{G}}{2\sigma}} \tag{14}$$

so that the critical value for the liquid pressure (12) is then

$$p_c = p_v - \sqrt[3\kappa-1]{\frac{(2\sigma)^{3\kappa}}{3\kappa\tilde{G}}}\left(1 - \frac{1}{3\kappa}\right). \tag{15}$$

On combining (14) and (15) the Blake critical radius is then given in the familiar form by

$$R_c = \frac{2\sigma}{(p_v - p_c)}\left(1 - \frac{1}{3\kappa}\right). \tag{16}$$

Note that

$$\begin{aligned} p_\infty - p_v &= \frac{2\sigma}{3R_0}\left(\frac{R_c}{R_0}\right)^2 - \frac{2\sigma}{R_0} \\ &= \frac{2\sigma}{3\kappa R_0}\left(1 - 3\kappa + \epsilon + \frac{1}{2}\frac{3\kappa}{3\kappa - 1}\epsilon^2 + \mathcal{O}\left(\epsilon^3\right)\right), \end{aligned} \tag{17}$$

and similarly

$$p_c - p_v = \frac{2\sigma(3\kappa - 1)}{3\kappa R_0}\left(1 - \frac{\epsilon}{2}\right)^{-1} \tag{18}$$

so the critical pressure p_c and the ambient pressure p_∞ in general differ by terms $\mathcal{O}(\epsilon)$ but when isothermal $\mathcal{O}(\epsilon^2)$. Thus when the equilibrium radius is close to the critical radius and the ambient pressure is close to the critical pressure, the natural frequency can be expressed as

$$\omega_0^2 = \frac{2\sigma\epsilon(3\kappa - 1)}{\rho R_0^3}. \tag{19}$$

When the perturbation is applied to the Rayleigh-Plesset equation (9) in this regime both the $\mathcal{O}(1)$ and $\mathcal{O}(\epsilon)$ terms are zero *if and only if the system is isothermal*, i.e. $\kappa = 1$. Thus, when isothermal to $\mathcal{O}(\epsilon^2)$ the governing equation is a Helmholtz oscillator

$$\ddot{x} + 2\zeta\dot{x} + x(1 - x) = \sum_{n=1}^{N} A_n \sin(\Omega_n(\tau + \tau_0)), \tag{20}$$

where the overdot represents the derivative with respect to the nondimensional time τ and

$$\zeta = \mu\sqrt{\frac{2}{\epsilon\sigma\rho R_0}}, \quad A_n = \frac{P_n R_0}{2\sigma\epsilon^2} \quad \text{and} \quad \Omega_n = \omega_n\sqrt{\frac{\rho R_0^3}{2\sigma\epsilon}}$$

are constant terms of $\mathcal{O}(1)$ when ϵ is small for bubbles whose initial radius is of order microns driven by frequencies in the megahertz range [11]. Here ζ is the nondimensional damping, Ω_n are harmonics of the nondimensional frequency, A_n the nondimensional Fourier components of the applied pressure and τ_0 is the phase of the incident wave. Note that the series expansion is truncated to N terms in order to disregard terms which are greater than $\mathcal{O}(\epsilon^2)$.

When forcing and viscosity are rescaled as small parameters, $\zeta \mapsto \varepsilon\zeta$ and $f \mapsto \varepsilon f$, which both destroy the integrable Hamiltonian structure then the Mel'nikov integral can be calculated. Let the ε-perturbed system be given by $\dot{\boldsymbol{x}} = \boldsymbol{f}_0(\boldsymbol{x}) + \varepsilon\boldsymbol{f}_1(\boldsymbol{x}, \tau)$ with $\boldsymbol{x} = (x, y)^T = (x, \dot{x})^T$ and $\boldsymbol{f}_1$ an Ω-periodic function. Explicitly the vector field is given by

$$\begin{aligned} \dot{x} &= y, \\ \dot{y} &= x(x - 1) + \varepsilon\left(\sum_{n=1}^{N} A_n \sin(\Omega_n\tau) - 2\zeta y\right). \end{aligned}$$

The unperturbed system, $\varepsilon = 0$, admits a homoclinic orbit $\boldsymbol{\gamma}$ emanating from the saddle at $(1, 0)$ of the form

$$\boldsymbol{\gamma}(\tau) = \frac{1}{2}\left(\tanh^2\left(\frac{\tau}{2}\right) - 1, 3\tanh\left(\frac{\tau}{2}\right)\operatorname{sech}^2\left(\frac{\tau}{2}\right)\right).$$

The first order Mel'nikov integral at the homoclinic energy level h can simply be calculated using Cauchy's residue theory as

$$\begin{aligned} \mathcal{M}(\tau_0) &= \int_{-\infty}^{+\infty} \boldsymbol{f}_0(\boldsymbol{x}) \wedge \boldsymbol{f}_1(\boldsymbol{x}, \tau + \tau_0)\, \mathrm{d}\tau \\ &= 6\pi\sum_{n=1}^{\infty} \frac{A_n\Omega_n^2}{\sinh(\Omega_n\pi)}\cos(\Omega_n\tau_0) - \frac{12\zeta}{5}. \end{aligned} \tag{21}$$

Due to the summation, it is not possible to formulate an explicit condition for simple zeros, but instead perform a calculation numerically. For both the Fubini and the Fay solutions it is simple to show numerically that the Mel'nikov integral has simple zeroes for larger A_n than in the case of linear wave propagation.

For the Fubini solution as $r_s \to 0$ the linear result is recovered and no summation is required, that is as $r_s \to 0$ so $P_1 \to P$, $P_j \to 0$ for all $j = 2, 3, \ldots$. As the distance towards the shock decreases, i.e. r_s increases from zero, so a higher P or larger R_0 is necessary in order for the Mel'nikov integral to have simple zeroes.

For the Fay solution higher pressures are required further from the shock. Also, higher pressures are required for materials with low Gol'dberg numbers than for materials with high Gol'dberg numbers.

A Poincaré section can be constructed which is topologically conjugate to a Bernoulli shift map on two symbols so that the likelihood of, say, $R_{\max}$ being greater or smaller than the previous cycle is as random as the toss of a coin. Thus, for sufficiently small ε, chaotic bubble oscillations will occur in the vicinity of $\boldsymbol{\gamma}$. From the simplified normal form, the effect of nonlinear wave propagation implies that a cascade to chaos and unbounded bubble growth will occur at higher driving pressures P or larger initial radii R_0 than for linear wave propagation. As $\Omega \to \infty$ then $\mathcal{M} \to 12\zeta/5$ and higher order contributions vanish, so that the stable and unstable manifolds stay disjoint. However, as $\Omega \to 0$ then $\mathcal{M} \to 12\zeta/5$, but now second order terms will affect the threshold criteria [18]. Indeed, numerical analysis suggests that higher order contributions must be taken into account in this regime. Furthermore, the authors [18] state that higher-order Mel'nikov analysis, i.e. a second aproximation of the separation distance between the stable and unstable manifolds is always necessary when considering nonlinear wave propagation due to the interactions of the differing harmonic excitations. Note that the classical first order Mel'nikov integral will typically overestimate the threshold by not including higher order contributions.

It is simple to show that in the absence of (nondimensional) viscous damping, i.e. $\zeta = 0$, that generically the Mel'nikov integral will have simple zeros for all (non-zero) parameter values. The effect of viscosity actually reduces the likelihood of violent cavitation, a result also found by Szeri [10]. No such analysis has yet been performed in the visco-elastic case but it is currently under investigation.

The bifurcation diagrams presented in figures 3 and 4 were computed for the Rayleigh-Plesset equation (9) with an adaptive, explicit Runge-Kutta method of order $(8, 5)$ with error control due to Dormand and Prince [19]. In order to ignore transient behaviour the first fifty cycles were disregarded and the next fifty cycles plotted. Figure 3 generalises the inferences from the radius-time profiles displayed in figure 2. Subfigure 3(a) illustrates that the maximum amplitude of the bubbles under forcing from nonlinear wave propagation is smaller than the maximum amplitude of bubbles under forcing from linear wave propagation. By defining ξ as the phase of the minimum radius $R_{\min} = R(t_{\min})$ per acoustic cycle [13]

$$\xi = (t_{\min} - t)/\Omega$$

subfigure 3(b) illustrates that inertial cavitation occurs earlier in each acoustic cycle for nonlinear waves than for linear waves. Both bifurcation diagrams in figure 3 show the same regions of developing instability for linear waves (illustrated by the dotted lines) as both solution measures determine Poincaré sections tangential to the motion of the cavity, i.e. when $\dot{R} = 0$.

Figure 4 shows a bifurcation diagram beyond the critical threshold and figure 5 then shows a selection of associated radius-time profiles illustrating the cascade to chaos through a period doubling bifurcation. Subfigure 5(a) shows a stable one-period radius-time profile at $P = 1.30$atm, which undergoes a period doubling bifurcation so that at $P = 1.35$atm in subfigure 5(b) the profile is two-periodic. For $P = 1.375$atm as subfigure 5(c) illustrates the radius-time profile is four-periodic. By $P = 1.40$atm the pressure has passed an accumulation point of period doubling bifurcations and as subfigure 5(d) illustrates the bubble oscillations are chaotic. Note that the pressure intervals between periodic cycles decreases as the system approaches chaotic oscillations, characteristic of the cascade to chaos. From a clinical perspective, when the duty cycle maybe in the order of seconds rather than micro seconds, accurate

predictions for the heat deposition on tumour sites over all but the shortest time scales can not be inferred from cavitation activity when the driving pressure is beyond the threshold.

Bifurcation diagrams of linear, see for example [13, figure 5], and nonlinear wave propagation, such as in figure 4, at equal driving pressures far beyond the threshold are significantly different, with differing regions of stability, indicating that beyond the threshold predictions based on inaccurate wave propagation models will be inaccurate for all but the shortest time.

5. Conclusion

In this paper the effect of nonlinear wave propagation of high intensity focused ultrasound on the stability of cavitating bubbles has been investigated numerically and analytically. The effect of nonlinear wave propagation redistributes energy from the primary harmonic to higher harmonics. From this two significant conclusions can be drawn; firstly the maximum bubble radius is reduced. This is clearly illustrated by the bifurcation diagram in subfigure 3(a). Thus the likelihood of shape instability is reduced. Secondly, inertial cavitation occurs earlier in each cycle, as illustrated by the bifurcation diagram in subfigure 3(b). The earlier onset of collapse allows for the bubble to return to an equilibrium radius and for inertial cavitation to reoccur.

Amongst the many threshold criteria applied to cavitation, it is worthwhile emphasising that although the Mel'nikov criteria does not exactly correspond to the escape boundary whereby bubbles increase without bound, it initiates the penetration of escaping tongues into the safe basin and therefore constitutes the first event in a well known sequence of complicated events which leads to unbounded bubble growth [20]. Thus the Mel'nikov criteria provides a lower bound threshold value. In the context of therapeutic applications, where safety is paramount, such a criterion is of great value.

In therapeutic applications a cloud of bubbles, comprised of many thousands of bubbles of differing equilibrium radii and resonance frequencies will be present, rather than a single, isolated bubble. Thus it could be assumed that a stability criterion for a single bubble is of limited use. However, the stability of a single bubble does provide insight into the stability of entire bubble clouds: experimental evidence [21] suggests that entire bubble clouds undergo period doubling cascade to chaos, not just the subset of bubbles which satisfy the Mel'nikov criterion. It is believed that the interaction between the bubbles results in an averaged behaviour. Indeed, numerical and experimental of the dimension of the attractor in phase space are remarkably low, between 2 and 2.5, indicating that the number of relevant degrees of freedom in the system is also low [22, 23].

In many applications of therapeutic ultrasound the tissue will have distributed inhomogeneities, leading to dissipation through diffraction, but it is conjectured that material nonlinearity is of greater significance than material inhomogeneity [24], although this subject is currently under investigation.

Acknowledgments

This work was supported under grant EP/F025750/1 and is gratefully acknowledged. The authors would like to thank S. Martynov, G. Vilensky and P. Gélat for insightful comments and discussions.

References

[1] Picinbono G, Delingette H and Ayache N 2001 Nonlinear and anisotropic elastic soft tissue models for medical simulation *Robotics and Automation, 2001. Proceedings 2001 ICRA. IEEE International Conference on* vol 2 (IEEE)
[2] Muir T G and Carstensen E L 1980 *Ultrasound Med. Biol.* **6** 345–57
[3] Humphrey V F 2000 *Ultrasonics* **38** 267–272
[4] Lauterborn W 1976 *J. Acoust. Soc. Am.* **59** 283–293
[5] Moss W C 1997 *J. Acoust. Soc. Am.* **101** 1187–1190

[6] Lauterborn W and Cramer E 1981 *Phys. Rev. Lett.* **47** 1445–1448
[7] Smereka P, Birnir B and Banerjee S 1987 *Phy. Fluids* **30** 3342–3350
[8] Guckenheimer J and Holmes P J 1983 *Nonlinear Oscillations, Dynamical systems, and Bifurcations of Vector Fields* (*Applied Mathematical Sciences* no 42) (New York, NY: Springer-Verlag)
[9] Chang H C and Chen L H 1986 *Phy. Fluids* **29** 3530–3536
[10] Szeri A J and Leal L G 1991 *Phy. Fluids* **3** 551–555
[11] Harkin A, Nadim A and Kaper T J 1999 *Phy. Fluids* **11** 274–287
[12] Kang I S and Leal L G 1990 *J. Fluid Mech.* **218** 41–69
[13] Simon G, Cvitanovic P, Levinsen M T, Csabai I and Horvath A 2002 *Nonlinearity* **15** 25–43
[14] Blackstock D T 1966 *J. Acoust. Soc. Am.* **39** 1019–1026
[15] Mitome H 1989 *J. Acoust. Soc. Am.* **86** 2334–2338
[16] Leighton T G 1994 *The Acoustic Bubble* (London: Academic Press)
[17] Brenner M P, Lohse D and Dupont T F 1995 *Phys. Rev. Lett.* **75** 954–957
[18] Lenci S and Rega G 2004 *Math. Probl. Eng.* **2004**(2) 145–168
[19] Hairer E, Nørsett S P and Wanner G 1993 *Solving ordinary differential equations I: Nonstiff problems* (*Springer Series in Computational Mathematics* no 8) (Berlin: Springer-Verlag)
[20] Thompson J M T 1989 *Proc. R. Soc. Lond. A* **421** 195–225
[21] Lauterborn W and Koch A 1987 *Phys. Rev. A* **35** 1974–1976
[22] Lauterborn W and Holzfuss J 1986 *Phys. Letts. A* **115** 369–372
[23] Holt R G, Gaitan D F, Atchley A A and Holzfuss J 1994 *Phys. Rev. Lett.* **72** 1376–1379
[24] Duck F A 1990 *Physical Properties of Tissue: A Comprehensive Reference Book* (London: Academic Press)

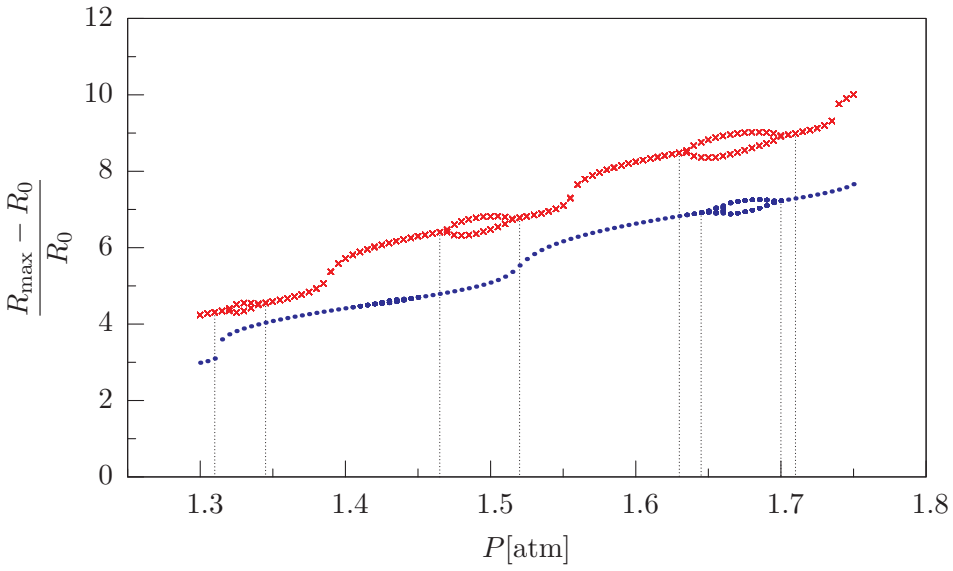

(a)

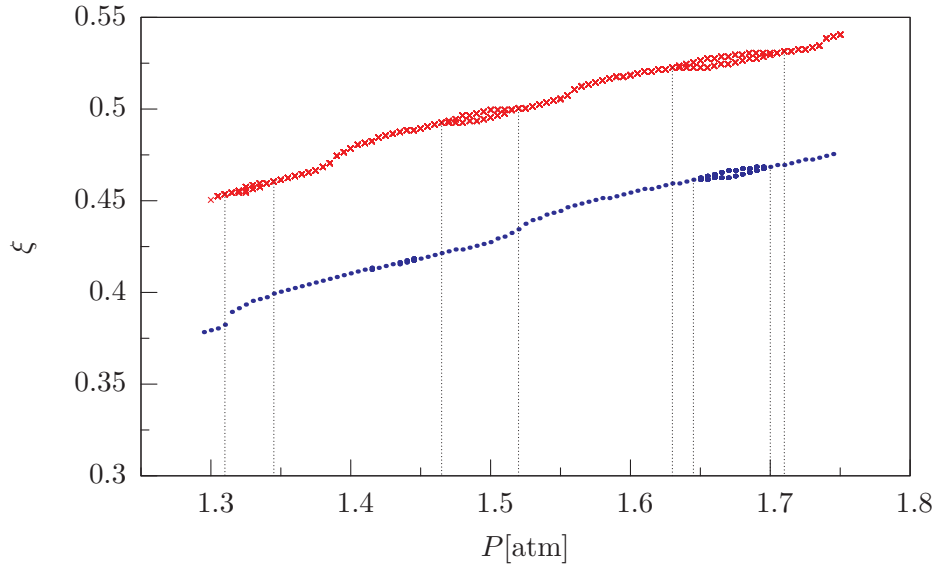

(b)

Figure 3. Bifurcation diagrams for a bubble determined by the Rayleigh-Plesset equation (9) with parameters given in figure 2 but with initial radius $R_0 = 0.9\mu$m. In both subfigures data from the fifty cycles is omitted in order to disregard transient behaviour. The radii from linear wave propagation are shown as red crosses, those from nonlinear wave propagation shown in blue dots. Subfigure 3(a) shows the change in the maximum amplitude, whereas subfigure 3(b) shows the change in the phase of the collapse, but the same qualitative features are displayed, that is period doubling bifurcations occur for lower pressures for linear waves than nonlinear waves.

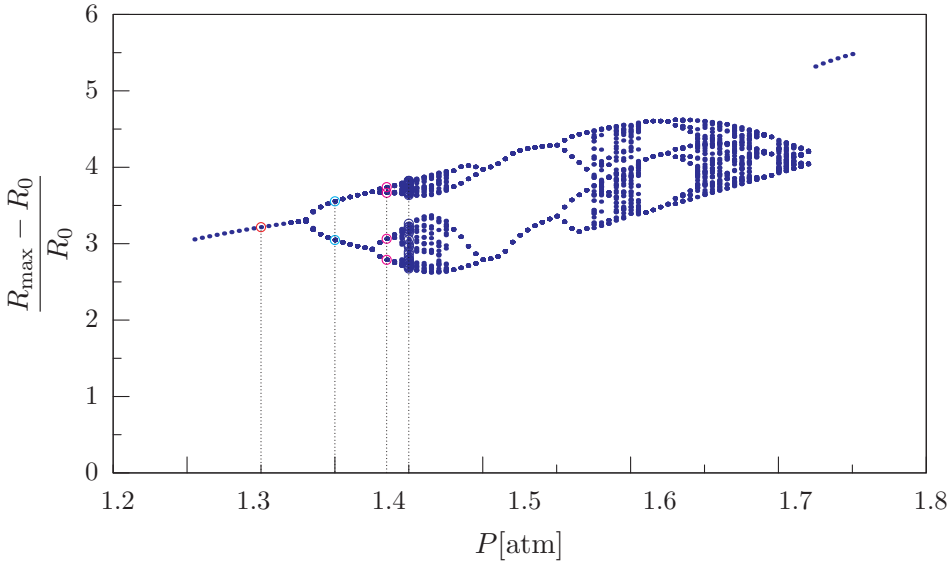

Figure 4. Bifurcation diagram showing the period doubling and the onset of quasi-periodic oscillations as the magnitude of the forcing pressure of the Fubini solution (5) is varied for the Rayleigh-Plesset equation (9). The parameters are the same as figure 3 except that now $R_0 = 1.4\mu$m. Profiles of the radius time curves at the marked pressures are illustrated in figure 5.

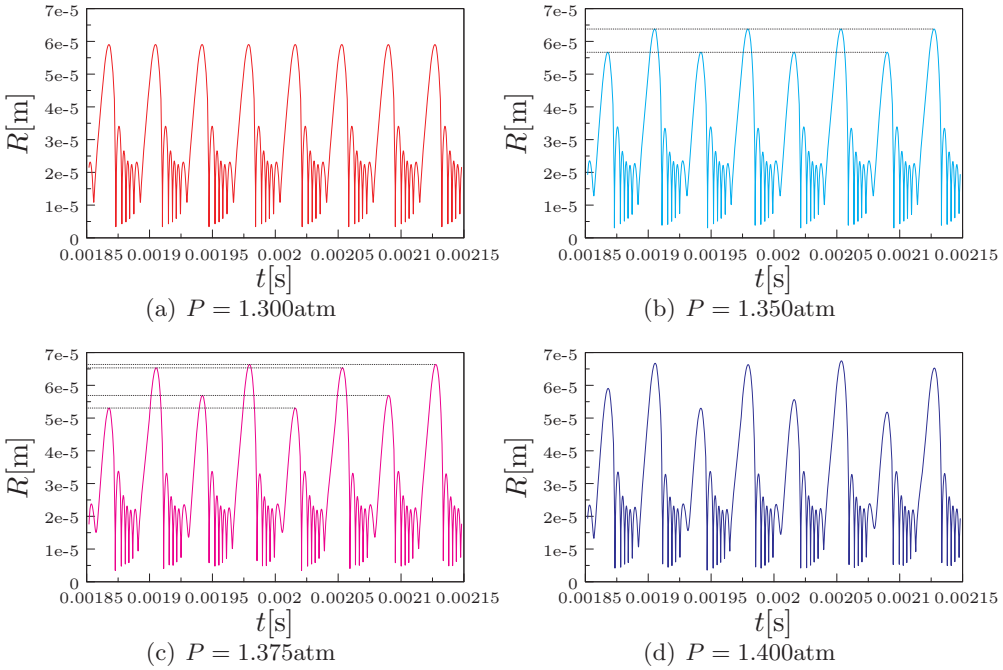

(a) $P = 1.300$atm (b) $P = 1.350$atm

(c) $P = 1.375$atm (d) $P = 1.400$atm

Figure 5. Period-doubling cascade to chaos as illustrated by the four subfigures marked on the bifurcation diagram 4. Subfigure 5(a) shows a stable one-period radius-time profile at $P = 1.30$atm, which undergoes a period doubling bifurcation so that at $P = 1.35$atm in subfigure 5(b) the profile is two-period. For $P = 1.375$atm as subfigure 5(c) is four period before subfigure 5(d) shows a chaotic profile at $P = 1.40$atm.